Available online at www.sciencedirect.com
SCIENCE DIRECT®
International Journal of Heat and Mass Transfer 48 (2005) 2126–2139
International Journal of HEAT and MASS TRANSFER
www.elsevier.com/locate/ijhmt

Optimal design of heat exchangers using the progressive quadratic response surface model

Kyoungwoo Park [a,*], Seungjae Moon [b,1]

[a] Department of Mechanical Engineering, Hoseo University, 29-1 Sechul-ri, Asan, Chungnam 336-795, Korea
[b] School of Mechanical Engineering, Hanynag University, 17 Haengdang-dong, Sungdong-gu, Seoul 133-791, Korea

Received 15 August 2004; received in revised form 31 December 2004
Available online 2 March 2005

Abstract

The optimal values of the design variables which minimize the pressure loss under the required temperature rise are obtained numerically in a plate-fin heat sink. In thermal/fluid systems, three fundamental difficulties such as a high computational cost for function evaluations (i.e., pressure drop and thermal resistance), the absence of design sensitivity information, and the occurrence of numerical noise are commonly confronted. Thus, sequential approximate optimization (SAO) algorithms have been used to overcome the above mentioned problems. In the present work, the progressive quadratic response surface method (PQRSM), which is one of the SAO algorithms, is proposed for constrained nonlinear optimization problems and is coupled with the computational fluid dynamics (CFD) for the optimization of heat sink. The optimal solutions obtained from the PQRSM are also compared with those of the sequential quadratic programming (SQP) method, which is one of the gradient-based optimization algorithms, to validate the efficiency and fidelity of the PQRSM.

Keywords: Heat exchanger; Optimization; Computational fluid dynamics; PQRSM

1. Introduction

Electronic equipments generally use heat sinks as cooling devices in order to effectively control heat arising from them. The heat sinks are commonly installed in the restricted space of the systems and their thermal performance can be improved both by enhancing the heat transfer rate and by reducing the pressure loss. Moreover, the advancement of packaging technologies has led the size of heat sinks miniaturized. Therefore, the optimal design of heat sinks is becoming more and more important issue and is one of interesting research areas in mechanical engineering; thereby it has been much paid attention by numerous researchers [1–4].

The optimal design of fluids/thermal (FT) systems associated with conventional optimization techniques such as a gradient-based algorithm requires not only a very difficult work, but also a high computational cost. However, the analysis of flow and thermal characteristics by the computational fluid dynamics (CFD) needs

* Corresponding author. Tel.: +82 2 2290 1639; fax: +82 2 2291 4070.
E-mail addresses: kwoopark@hanyang.ac.kr (K. Park), smoon@hanyang.ac.kr (S. Moon).
[1] Tel.: +82 2 2290 0450.

0017-9310/$ - see front matter © 2005 Elsevier Ltd. All rights reserved.
doi:10.1016/j.ijheatmasstransfer.2004.12.023

Nomenclature

a_{ij}	coefficients of approximate function
B_1, B_2	base- and lower-part of fin width [m]
$\mathbf{B}_k$	Hessian matrix
c_0	coefficient of approximate function
C_1, C_2, C_3, C_λ, C_μ	empirical constants in the k–ε model
$\mathbf{D}_k$	second-order of quadratic approximation model
$f(\mathbf{x})$	objective function
$\tilde{f}(\mathbf{x})$	approximation of $f(\mathbf{x})$
f_R, f_λ	empirical functions in the k–ε model
$g_j(\mathbf{x})$	inequality constraints
$\tilde{g}_j(\mathbf{x})$	approximation of $g_j(\mathbf{x})$
$\mathbf{g}_k$	first-order of quadratic approximation model
G_b, G_k	generation terms in the k–ε model
$\tilde{\mathbf{G}}_k$	normalized approximate Hessian matrix
h	fin height [m]
H	height of heat sink (=$h + t$), [m]
k	turbulent kinetic energy [m^2/s^2]
k_s	thermal conductivity for solid [W/m K]
L	length [m]
n	number of design variables
P	pressure [Pa]
ΔP	pressure drop [Pa]
Q	dissipated heat [W]
r^k	trust region ratio
$\mathbf{S}_k$	diagonal matrix
t	base thickness of heat sink [m]
T, T'	mean and fluctuating temperature, respectively [K]
ΔT	temperature rise [K]
u_j, u'_j	mean and fluctuating velocities, respectively [m/s]
W	width [m]
x, y, z	Cartesian coordinates [m]
$\mathbf{x}$	design variable vector

Greek symbols

ε	dissipation rate of k [m^2/s^3]
θ_j	thermal resistance [K/W]
μ, μ_t	viscosity and eddy viscosity [N s/m^2]
ρ	density [kg/m^3]
σ_k, σ_ε	turbulent Prandtl and Schmidt number for k and ε
ϕ	general dependent variable
Γ_k	radius of trust region

Subscripts

E	exit
H	heat sink
hs	heat source
in	inlet
j	junction or maximum
k	number of iteration
R	reactor
∞	ambient

Superscript

*	approximate optimal points

an excessive CPU time for computing the objective functions for heat transfer rate and pressure drop. Thus, approximation models such as the sequential approximate optimization (SAO) technique have been introduced into the optimization of FT-system. The SAO technique optimizes the approximate problems iteratively until the convergence criteria are satisfied. Generally, the SAO is classified into two categories according to information required during the optimization: gradient-based approximation (GBA) and function-based approximation (FBA). In the GBA, gradient information for objective functions and/or constraints are required to approximate the optimization problem. However, it is often unavailable and sometimes too expensive to approximate through the finite difference method because the analysis of design sensitivity has to be performed. Thus, in particular optimization problems the GBA cannot be applicable to optimize the FT-system. In contrast to the GBA, the FBA only needs the function for optimization and is relatively simple in the approximate optimization problem. The most widely used methodology in the FBA is the response surface approximation (RSA) [5,6] related to the trust region algorithm and the design of experiments. The RSA, which is originally developed for constructing the global optimization, does not need the procedure of sensitivity analysis so that it is a suitable method in this considered study. In addition, the RSA is an adequate method in FT-systems which frequently encounters the numerical noise because it can give the smoothness of response, thereby avoiding local or sub-optimal solutions in a wide range of design spaces. However, the main difficulty faced by the RSA is that it requires a large number of the design points through design of experiments (or the number of necessary function analyses) to construct a response surface for a function that involves the design variables n. For example, for the conventional quadratic response models, the computational requirements grow by the square of the number of the design variables (i.e., $(n + 1) \cdot (n + 2)/2$ terms).

In order to construct an approximate model efficiently even though the problem has a large number of design variables, researchers in the *i*DOT (*the center of innovative design optimization technology*, in Hanyang University) [7,8] have proposed the progressive quadratic response surface model (PQRSM) and applied it to the MDO (multidisciplinary design optimization) problem. The PQRSM has the following two merits: Firstly, it requires only $(2n + 1)$ points for determining the regression coefficients of linear and quadratic terms in each approximation. The two-factor interaction terms are also determined by using the normalized quasi-Newton formula. Moreover, it algorithmically converges from the global quadratic to the local approximations in the context of the trust region model management strategy. Secondly, the PQRSM does not require the additional CPU time to explicitly construct a quadratic approximate model because it uniquely determines all the regression coefficients and updates the remained regression coefficients for the two-factor interaction terms using the uniquely determined terms.

In this study, the optimal values of the design variables of a plate-fin type heat sink are numerically obtained using the CFD associated with the PQRSM in order to minimize the pressure drop under the required temperature rise. The overall procedure including the analysis of flow/thermal fields and the optimization is carried out through the batch-job process. The efficiency of the PQRSM is also investigated by comparing the optimized solutions with those of the sequential quadratic programming (SQP) method which is a gradient-based local optimization technique.

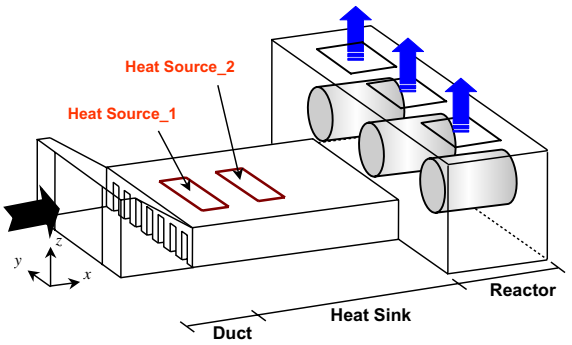

Fig. 1. Schematic diagram of thermal system and coordinate system.

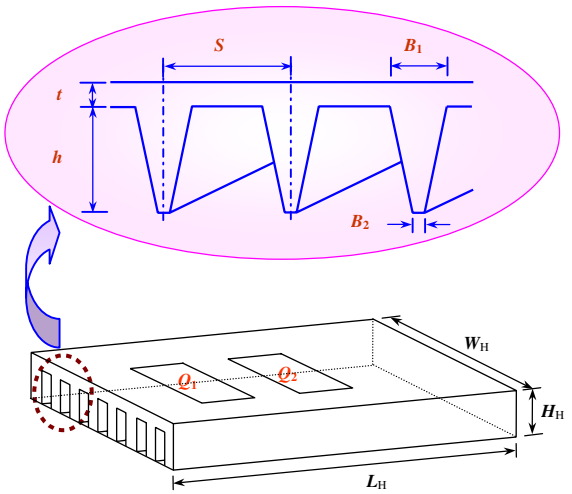

Fig. 2. Plate-fin type heat sink.

2. Definition of optimization problem

2.1. Physical model

A thermal system under consideration for optimization is a fan-drive heat sink with plate-fins consisting of duct, heat sink, and reactor and is illustrated schematically in Fig. 1. Air induced by an axial fan (Model: 3112KL-05 W-B50, size: $32 \times 80 \times 80$ mm, Max. flow rate: 1.46 m^3/min) with a constant temperature (T_{in} = 318 K) passes the duct which plays a role of a flow guidance and enters the channels formed by fins and heat sink base. Thereafter, heated air, which absorbs the heat from the heat sink, flows out through exits (88×55,$L_E \times W_E$ mm, 3EA) located top wall of the reactor part. The overall dimension of reactor part is $160 \times 360 \times 150$ ($L_R \times W_R \times H_R$) mm and it contains three reactors. The temperature of each reactor is kept on 343 K and has a diameter of 75 mm and a length of 125 mm.

Fig. 2 depicts the detailed physical configuration of the plate-fins heat sink schematically because the objective of this study is to optimize the heat sink shape for high performance. The heat sink is made of aluminum (ρ = 2707 kg/m^3, k_s = 204 W/m K) and the fins are manufactured by extruding technique. The overall dimensions of a heat sink are a length L_H = 430 mm, a width of W_H = 188 mm, and a height of H_H = 65 mm. Noting that the height of the heat sink (H_H) is the sum of the fin height (h) and the base thickness of the heat sink (t). Two heat sources with projected heating areas of dimensions of 62×122 mm ($L_{hs} \times W_{hs}$), which are mounted on the top wall of the heat sink, uniformly generate the heat by two different electric resistance heaters (Q_1 = 348 W, Q_2 = 321 W) as shown in Fig. 2. The heat generated by heat sources is conducted through the heat sink at first and then it is rejected to the environment by means of forced convection. Thus, the problem considered becomes a conjugated heat transfer problem. Fig. 2 also shows that the internal shape of the heat sink

can be determined by geometrical parameters such as the fin pitch (S) or number of fins, base thickness of the heat sink (t) or fin height (h), base-part fin width (B_1), and lower-part fin width (B_2).

2.2. Optimization

2.2.1. Mathematical formula for optimization

Optimization problems are made up of the following basic ingredients; a set of design variables, a performance (or objective) function, a set of constraints, and side constraints. The optimization is to find values of the design variables that minimize or maximize the objective function numerically while satisfying the constraints. In this point of view, the nonlinear, constrained optimum design problem can be expressed mathematically as follows:

$$\text{Find} \quad \mathbf{x} = [x_1, x_2, \cdots x_n]^{\mathrm{T}} \tag{1}$$

$$\text{to minimize} \quad f(\mathbf{x}) \tag{2}$$

$$\text{subject to} \quad g_j(\mathbf{x}) \leqslant 0 \quad \text{for } j = 1, m \tag{3a}$$

$$x_i^{\mathrm{L}} \leqslant x_i \leqslant x_i^{\mathrm{U}} \quad \text{for } i = 1, n \tag{3b}$$

where $\mathbf{x}$ represents the design variable vector and n is the number of design variables. $f(\mathbf{x})$ is the objective function which depends on the values of the design variables. $g_j(\mathbf{x})$ denotes the inequality constraint. $\mathbf{x}_i^{\mathrm{L}}$ and $\mathbf{x}_i^{\mathrm{U}}$ are the lower and upper limits of the design variables, respectively, and they simply limit the region of search for the optimization. m is the number of constraints.

2.2.2. Objective functions and design variables

High performance of the heat sink can be easily achieved both by improving the heat transfer rate and by adopting the large capacity of a fan. For a given operating condition of a fan, increasing the heat transfer rate, however, is accompanied by increasing the pressure drop as a necessity. It is obvious from this phenomenon that a high thermal performance (or cooling efficiency) can be obtained both by minimizing the thermal resistance and the pressure drop in the case of fixed volume of the heat sink. The pressure drop (ΔP) and the thermal resistance (θ_j) have been generally adopted as the objective functions to be minimized in many industrial applications and they are given by

$$\theta_j = \frac{T_j - T_\infty}{Q}, \quad \Delta P = P - P_\infty \tag{4}$$

where T_j is the maximum or junction temperature, T_∞ the ambient temperature, and Q the heat generated through the heat sink. P and P_∞ are the average pressure in the heat sink and the ambient pressure, respectively.

As shown in Eq. (4), a number of different objectives often have to be minimized at once and is called a multi-objective optimization problem. Usually, the different objectives such as pressure drop and heat transfer rate are not compatible, that is, the variables that optimize one objective may be far from optimal for the others. Therefore, the ways for treating a multi objective function problem have been introduced; optimization problems with multiple objectives are reformulated as single-objective problems by either forming a weighted combination of the different objectives or else replacing some of the objectives by constraints. In a practical situation for a heat sink design, it is generally required that the maximum temperature (or temperature rise, ΔT) should be maintained under the desired one. Thus, the maximum temperature (or ΔT) is used as a constrained condition and the pressure drop is adopted as an objective function only in this study.

The geometric parameters which strongly influence the thermal performance of the heat sink are the base-part fin width (B_1), lower-part fin width (B_2), and base thickness of heat sink (t), as depicted in Fig. 2. Thus, three design variables are considered in this study: $x_1 = B_1$, $x_2 = B_2$, and $x_3 = t$ (i.e., $\mathbf{x} = [B_1, B_2, t]$).

3. Mathematical optimization

3.1. Sequential approximate optimization (SAO)

Often, a high computational cost is arising from evaluating objective functions in FT-systems related to the computational fluid dynamics. It is also commonly encountered that the responses of the system analysis are discontinuous or numerical noise. Thus, the responses should be formed as smooth functions in a design optimization process. In addition, gradient-based optimization techniques such as the SQP and SLP methods need derivative information for obtaining the objective function minimized, which is related to Navier–Stokes equation. However, it is often not available and it is very difficult to conduct the sensitivity analyses in FT-systems. The use of approximation technologies for optimization has been recommended such as the response surface approximation (RSA) to overcome these problems. It has grown in interest in recent years because it does not require the design sensitivity. In the RSA, a sequential approximate optimization (SAO) strategy, in which an optimization for an approximate problem is iteratively repeated until convergence, has been commonly used.

The optimization problem is approximated by the following equations and then solved by means of a SAO method.

$$\text{minimize} \quad \tilde{f}(\mathbf{x}), \quad \mathbf{x} = [x_1, \ldots, x_n] \tag{5}$$

$$\text{subject to} \quad \tilde{g}_j(\mathbf{x}) \leqslant 0, \quad j = 1, m \tag{6}$$

$$\max[\mathbf{x}_{\mathrm{L}}, \mathbf{x}_{\mathrm{L}}^{(k)}] \leqslant \mathbf{x} \leqslant \min[\mathbf{x}_{\mathrm{U}}^{(k)}, \mathbf{x}_{\mathrm{U}}] \tag{7}$$

where the superscript $\sim$ means the approximated amount. The additional move limits ($\mathbf{x}_{\mathrm{L}}^{(k)}$ and $\mathbf{x}_{\mathrm{U}}^{(k)}$), as shown in Eq. (7), are controlled logically in SAO process to ensure the accuracy of approximation at the current design iteration, $\mathbf{x}^{(k)}$. They are temporally applied at each iteration and can be changed as the optimization proceeds within the global ranges of the design variables, $\mathbf{x}^{\mathrm{L}} \leqslant \mathbf{x} \leqslant \mathbf{x}^{\mathrm{U}}$.

3.2. Progressive quadratic response surface model (PQRSM)

The PQRSM used in this study constructs an approximate model by means of a way of the global optimization at first, and then obtains the accurate optimal values with a local optimization as the optimization proceeds. The PQRSM has the following three characteristics compared to the conventional response surface model; the choice of the initial design samples, the use of the normalized quasi-Newton formula for the quadratic approximation process, and the explicitly construction of approximate model without using a least square method.

3.2.1. The design sampling points

One of the important issues for constructing an accurate model is the choice of a proper set of sampling points for design of experiments. At the initial step ($\mathbf{x}_1^0$), total sampling points of $(2n+1)$ for each design variable (that is, two points along the axis ($2n$) and the center point (1)) are selected as shown in Fig. 3a. Then the quadratic approximate model is constructed using the three-point polynomial interpolation method after the exact function values are evaluated at the selected $(2n+1)$ points. That is, using the (x_0,f_0) for a center point and the (x_{i1},f_{i1}) and (x_{i2},f_{i2}) for two points along the axis in the ith design variable, the quadratic approximate function for the ith design variable, $\tilde{f}_i$ can be obtained as

$$\tilde{f}_i = a_{i0} + a_{i1}x_i + a_{i2}x_i^2 \tag{8}$$

where

$$a_{i2} = \frac{(f_{i2}-f_0)/(x_{i2}-x_0) - (f_{i1}-f_0)/(x_{i1}-x_0)}{x_{i2}-x_{i1}}$$

$$a_{i1} = \frac{f_{i1}-f_0}{x_{i1}-x_0} - a_{i2}(x_0+x_{i1})$$

$$a_{i0} = f_0 - a_{i1}x_0 - a_{i2}x_0^2$$

If the number of design variable is two, a three-point quadratic approximate function can be expressed as a matrix form as follows:

$$\tilde{f} = c_0 + \mathbf{C}^{\mathrm{T}}\mathbf{x} + \mathbf{x}^{\mathrm{T}}\mathbf{D}\mathbf{x} \tag{9}$$

where

$$c_0 = -(a_{11}+a_{21})x_0 - (a_{11}+a_{22})x_0^2$$

$$\mathbf{C} = \begin{bmatrix} a_{11} \\ a_{21} \end{bmatrix}, \quad \mathbf{D} = \begin{bmatrix} a_{11} & 0 \\ 0 & a_{22} \end{bmatrix}$$

A response surface model can be uniquely developed using the selected $(2n+1)$ points because the quadratic terms for the approximate model are only diagonal components. This approximate model is optimized within the initial trust region of $I^{(1)}$ and then new design of $\mathbf{x}_1^*$ is updated as shown in Fig. 3(a). Now, we evaluate the exact function value for $\mathbf{x}_1^*$ and check the accuracy

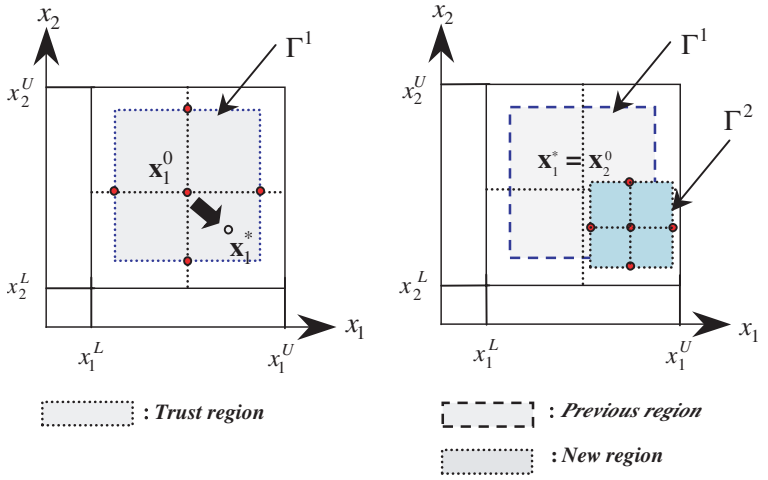

(a) At the 1st iteration **(b)** At the 2nd iteration

Fig. 3. Design points sampling at first two iterations.

of approximation using the trust region ratio (r^k), which will be discussed later, and then adjust the new trust region of $\Gamma^{(2)}$ for the next iteration. The sampling points for the region of $\Gamma^{(2)}$ are selected around an approximate optimal point ($\mathbf{x}_1^* = \mathbf{x}_2^0$) as shown in Fig. 3(b) and a new quadratic approximate model is constructed in the same way as the first iteration step. In the trust region model, the optimization problem is solved at around $\mathbf{x}^k$ for the kth iteration step. In this case, the move limits of Eq. (7) are defined by means of a radius of trust region, $\Gamma^{(k)}$.

$$\left\|\mathbf{x} - \mathbf{x}^k\right\|_p \leqslant \Gamma^k \tag{10}$$

where the p norm defines the shape of the region and the hyper-cubic type is used in this study. The hyper-cubic type trust region can easily present a sub-region when design points are active to their lower and upper limits, while the hyper-spherical type trust region cannot [7].

The trust region algorithm was originally developed to apply to the nonlinear unconstrained optimization problem with a robust global behavior [9]. The quadratic approximate function, Eq. (8), is successively minimized with the controlled trust region in each iteration. The size of the trust region in Eq. (10), $\Gamma^{(k)}$ should be controlled based on how well the quadratic model predicts the decrease in $f(\mathbf{x})$. In the PQRSM, the trust region is adjusted using a new variable introduced, r^k which is called the trust region ratio and is given by

$$r^k = \frac{\Delta f_k}{\Delta \tilde{f}_k} = \frac{f(\mathbf{x}_k) - f(\mathbf{x}_{k+1}^*)}{\tilde{f}(\mathbf{x}_k) - \tilde{f}(\mathbf{x}_{k+1}^*)} \tag{11}$$

where $\mathbf{x}_{k+1}^*$ denotes the new design points. This equation implies the ratio of the actual change (or reduction) in $f(\mathbf{x})$ to the corresponding predicted change by the approximation at the kth-iteration. That is, the closer r^k is to unity, the better the agreement is. The trust region algorithm is the best model management in an approximate optimization because it adaptively reduces $\Gamma^{(k)}$ to maintain a certain degree of agreement as measured by r^k. If r^k is greater than unity, the new design points $\mathbf{x}_{k+1}^*$ is considered as $\mathbf{x}_{k+1}$ and the radius of trust region is updated according to the following equation as

$$\Gamma^k = \begin{cases} \gamma_0 \Gamma^{k-1} & \text{if } 0 < r^k < \varepsilon_1 \\ \gamma_1 \Gamma^{k-1} & \text{if } \varepsilon_1 < r^k < \varepsilon_2 \\ \gamma_2 \Gamma^{k-1} & \text{if } r^k \geqslant \varepsilon_2 \end{cases} \tag{12}$$

where $\gamma_0 = 0.25,\ \gamma_1 = 1,$

$$\gamma_2 = \begin{cases} 2 & \text{if } \|x^* - x^0\| = \Gamma^k, \\ 1 & \text{if } \|x^* - x^0\| < \Gamma^k, \end{cases} \quad \varepsilon_1 = 0.25, \quad \varepsilon_2 = 0.75$$

It is noted that from the second-iteration, the optimization is carried out not by using the simplified quadratic function obtained in Eq. (8), but by using the normalized quasi-Newton method, which will be explained in detail in the next section.

3.2.2. Normalized quasi-Newton formula

The conventional quasi-Newton Hessian updated formula use only a local information between consecutive iterations throughout the optimization process, whereas the PQRSM uses the normalized quasi-Newton method [7].

Let $\mathbf{g}_k$ and $\mathbf{D}_k$ be the regression coefficients of the first- and second-orders in the quadratic approximation equation of Eq. (8) at the kth-iteration, which is approximated using design points of $(2n + 1)$. The approximate Hessian at the kth-iteration, $\mathbf{B}_k$ can be constructed using the quasi-Newton formula, which is well known as the BFGS method [9].

$$\mathbf{B}_k = \mathbf{B}_{k-1} - \frac{(\mathbf{B}_{k-1}\boldsymbol{\delta}_k)(\mathbf{B}_{k-1}\boldsymbol{\delta}_k)^{\mathrm{T}}}{\boldsymbol{\delta}_k^{\mathrm{T}}\mathbf{B}_{k-1}\boldsymbol{\delta}_k} + \frac{\mathbf{y}_k\mathbf{y}_k^{\mathrm{T}}}{\mathbf{y}_k^{\mathrm{T}}\boldsymbol{\delta}_k} \tag{13}$$

where $\boldsymbol{\delta}_k = \mathbf{x}_k - \mathbf{x}_{k-1}$ and $\mathbf{y}_k = \mathbf{g}_k - \mathbf{g}_{k-1}$. For an initial condition, $\mathbf{B}_1 = \mathbf{D}_1$. The original second-order term ($\mathbf{D}_k$) at the design point of $\mathbf{x}_k$ has no off-diagonal coefficients. However, a quasi-Newton formula, Eq. (13) mathematically gives the off-diagonal terms in $\mathbf{B}_k$. For smaller range of Γ^k, $\mathbf{D}_k$ has a more accurate diagonal information than $\mathbf{B}_k$ and this characteristic will be gradually dominated as the optimization proceeds. Thus, in order to replace the diagonal coefficients of $\mathbf{B}_k$ to $\mathbf{D}_k$, the following normalized approximate Hessian, $\tilde{\mathbf{G}}_k$ is used.

$$\tilde{\mathbf{G}}_k = \mathbf{S}_k^{\mathrm{T}}\mathbf{B}_k\mathbf{S}_k \tag{14}$$

Here $\mathbf{S}_k$ is the diagonal matrix and $\mathbf{S}_k^{ii}$, which is the ith component of $\mathbf{S}_k$, is defined as

$$\mathbf{S}_k^{ii} = \frac{\sqrt{|D_k^{ii}|}}{\sqrt{|B_k^{ii}|}} \tag{15}$$

The signs of diagonal coefficients in the normalized Hessian are replaced by those of $\mathbf{D}_k$. In the sufficiently small or well-established trust region, $\mathbf{D}_k$ and $\mathbf{g}_k$ within trust regions are almost equal to those of approximate differentials by means of the central difference method. This implies that $\tilde{\mathbf{G}}_k$ is nearly equal to the exact Hessian matrix at $\mathbf{x}_k$. Finally, Eq. (13) is modified as follows:

$$\mathbf{B}_k = \tilde{\mathbf{G}}_{k-1} - \frac{(\tilde{\mathbf{G}}_{k-1}\boldsymbol{\delta}_k)(\tilde{\mathbf{G}}_{k-1}\boldsymbol{\delta}_k)^{\mathrm{T}}}{\boldsymbol{\delta}_k^{\mathrm{T}}\tilde{\mathbf{G}}_{k-1}\boldsymbol{\delta}_k} + \frac{\mathbf{y}_k\mathbf{y}_k^{\mathrm{T}}}{\mathbf{y}_k^{\mathrm{T}}\boldsymbol{\delta}_k} \tag{16}$$

Eq. (16) is called as the normalized quasi-Newton formula in this study. Finally, the approximate model used in the PQRSM becomes

$$\tilde{f}(\mathbf{x}_k) = f(\mathbf{x}_{k-1}^*) + \mathbf{g}_k^{\mathrm{T}}(\mathbf{x}_k - \mathbf{x}_{k-1}^*) + \frac{1}{2}(\mathbf{x}_k - \mathbf{x}_{k-1}^*)^{\mathrm{T}}\tilde{\mathbf{G}}_k(\mathbf{x}_k - \mathbf{x}_{k-1}^*) \tag{17}$$

In the above equation, $\mathbf{g}_k^{\mathrm{T}}$ is obtained by the response surface approximation, while $\tilde{\mathbf{G}}_k$ can be acquired by means of both the RSM and the BFGS methods. In

the present work, the approximate model, $\tilde{f}(\mathbf{x}_k)$, at the trust region of the kth-iteration is minimized to obtain the optimal solutions by a local optimization technique of SQP method [10].

4. Numerical methodology

In order to obtain the optimal design parameters of the heat sink with plate-fins, the following three programs are used;

(1) the main program which defines various arrays and parameters,
(2) the analyzer that evaluates the objective functions, and
(3) the optimizer which can solve a nonlinear optimization problem.

Fig. 4 shows the flowchart of the numerical methodology for optimization. Once the objective function (Δp) are obtained as the results of calculation of flow and thermal fields by the analyzer, the main program calls the optimizer to proceed with optimization. The optimizer may modify the design variables. When the optimizer requires new values of the objective functions, it returns to the main program and the analyzer is called to calculate them. In this step, the analyzer should generate a new grid system because new design variables are proposed by the optimizer. This process is repeated until the optimization is complete and is performed automatically. As a result of optimization, the optimal design variables and the corresponding pressure drop is obtained.

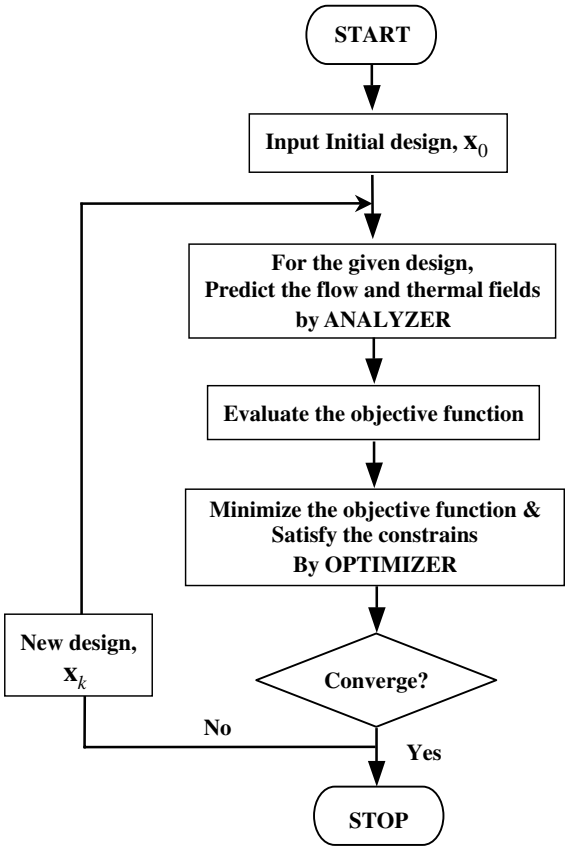

Fig. 4. Numerical methodology for optimization.

4.1. Flow and thermal fields

4.1.1. Mean flow equations

The physical problem considered in this study is the three-dimensional turbulent mixed convective flow and heat transfer of steady and incompressible fluid. The fluid properties are taken to be constant except for the density in the buoyancy terms of the momentum equation. The effects of viscous dissipation and radiation heat transfer are assumed to be negligibly small. Due to the symmetric geometry, the computation is only carried out one half of the physical domain. Using the above-mentioned assumptions, the Reynolds-averaged Navier–Stokes (RANS) equations for mass, momentum, and energy are solved.

4.1.2. Turbulent modeling

The RANS equations contains the Reynolds stress, $\overline{\rho u_i' u_j'}$ in the momentum equations and the turbulent heat flux, $\overline{\rho u_i' T'}$ in the energy equation, and they govern the turbulent diffusion which should be determined. In order to resolve the closure problem of the governing equations, the standard k–ε turbulence model proposed by Rodi [11] is introduced in this work. According to the eddy-viscosity concept, the turbulent kinetic energy (k) and its dissipation rate (ε) are obtained from the following transport equations:

$$\frac{\partial(\rho u_j k)}{\partial x_j} = \frac{\partial}{\partial x_j}\left[\left(\mu + \frac{\mu_t}{\sigma_k}\right)\frac{\partial k}{\partial x_i}\right] + G_k + G_b - \rho\varepsilon \tag{18}$$

$$\frac{\partial(\rho u_j \varepsilon)}{\partial x_j} = \frac{\partial}{\partial x_j}\left[\left(\mu + \frac{\mu_t}{\sigma_\varepsilon}\right)\frac{\partial \varepsilon}{\partial x_i}\right] + C_1\frac{\varepsilon}{k}(G_k + C_3 G_b) - C_2\rho\frac{\varepsilon^2}{k} \tag{19}$$

where μ_t is the turbulent viscosity and is defined as $\mu_t = \rho C_\mu k^2/\varepsilon$. u_j the average velocities, G_k and G_b are the turbulent production terms of stress and buoyancy force, respectively. The model constants and various functions used in the k–ε model are found in Rodi [11] and Abe et al. [12].

4.1.3. Boundary conditions

We use the following boundary conditions to predict the flow and thermal fields in thermal system including the heat sink.

Inlet: The coolant of a constant temperature (T_{in} = 318 K) induced by an axial fan enters the system with a constant velocity (u_{in} = 1.27 m/s) and a swirl condition of 60 rad/s. The corresponding turbulent kinetic energy and its dissipation rate are calculated from the following formula: $k_{in} = 1.5I_0^2u_{in}^2$, $\varepsilon_{in} = k_{in}^{3/2}/L_\varepsilon$, where the local turbulence intensity, I_0 is assumed to be 0.1 and L_ε is a length scale for dissipation, taken here as 80 mm (fan width).

Outlet: The pressure boundary condition is imposed at the outflow plane. For the other variables, the Newmann condition is employed.

Solid surfaces: No-slip boundary conditions for all solid walls are assigned for velocity. For the turbulent kinetic energy and its dissipation rate, the wall function based on empirical wall law is employed. At the heat sink walls, the following thermal boundary conditions are imposed; Two different heat fluxes are uniformly applied to the heat sink at the top wall of the heat sink (62×122 mm) by two heat sources. At the side wall and the top wall except for heat sources, the convective boundary conditions are used (h = 3 W/m^2 K). At the bottom wall of heat sink, the adiabatic condition is adopted. The solid walls of the duct and reactor are assumed to be adiabatic.

Symmetric plane: Symmetric conditions are imposed for all dependent variables at the plane of symmetry (i.e., $y = 0$).

4.1.4. Numerical solution procedure

The governing equations for the three-dimensional turbulent flow and thermal fields are solved using FLUENT which is a commercial finite volume CFD code [13]. The reason for using the CFD code is as follows: to obtain the optimum design variables by means of the mathematical optimization technique, a fast and reliable computer program must be used because it operates repeatedly for many different geometrical configurations during the optimization process. All of the commercial CFD codes, however, basically solve the flow and thermal characteristics via the GUI. Thus, it is an important task to combine commercial CFD solver with mathematical optimization method in order to carry out the optimization automatically. In this study, we make the script files and re-solve the above mentioned problem. The SIMPLE algorithm [14] is used to calculate the pressure correction equation in the momentum equation. The power law scheme is employed for the treatment of convection and diffusion terms.

In the optimization problem, because a new shape of fins is proposed in every iterative step of the optimization process, a new grid system according to the modified design variables is required. Therefore, the number of cells for the computational domain has to be given sufficiently large (for baseline geometry, its number is around 1,300,000 cells) by considering the fine grid system at solid–gas interfaces.

When the results satisfy the following conditions simultaneously, the solutions are treated as converged ones:

$$R = \sum_{\text{domain}} |a_{nb}\phi_{nb} + b - a_P\phi_P| < 10^{-5}, \qquad \left|\frac{\phi_{k+1} - \phi_k}{\phi_k}\right| < 10^{-5} \tag{20}$$

where R represents the residual sum and ϕ is a general dependent. The subscripts k and nb are the number of iteration and the neighborhood grid points, respectively.

4.2. Optimization

The numerical procedure of optimization used in the trust model management strategy for the PQRSM effectively is shown in Fig. 5 as a flowchart and is explained briefly.

Step 0: The initial trust region is assumed to 30–50% for design space that includes the initial design values.

Step 1: Construct a quadratic model using a quadratic polynomial approximation along each design variable axes. Let their coefficients be $\mathbf{g}_k$ and $\mathbf{D}_k$ for linear and quadratic terms, respectively. If $(k + 1)$ then, go to Step 3, Otherwise, set $\mathbf{y}_k = \mathbf{g}_k - \mathbf{g}_{k-1}$.

Step 2: Evaluate the coefficient matrix of the second-order term ($\mathbf{B}_k$) using Eq. (16) and construct $\tilde{\mathbf{G}}_k$ by normalizing $\mathbf{S}_k^{\mathrm{T}}\mathbf{B}_k\mathbf{S}_k$.

Step 3: Minimize $\tilde{f}(\mathbf{x})$ in Eq. (17).

Step 4: Evaluate the actual and the predicted reductions such as $\Delta f_k(\mathbf{x})$ and $\Delta\tilde{f}_k(\mathbf{x})$ using Eq. (11). Then, check the trust region ratio r^k. If $r^k > 0$, then update $\mathbf{x}_k$ and go to Step 5 with $(k = k + 1)$. Otherwise, go to Step 3 with the reduced trust region using Eq. (12).

Step 5: If the convergence criteria are satisfied, then stop. In the PQRSM, the solutions are treated as the convergence ones when the following criteria are satisfied simultaneously as; (1) the relative or absolute deviation of objective functions between consecutive SAO iterations is less than 10^{-3}, and (2) the amount of maximum violation for constraints is less than 10^{-4}. Otherwise, select new $2n$ design points around $\mathbf{x}_{k+1}$, within the new trust region Γ^{k+1} and go to Step 1.

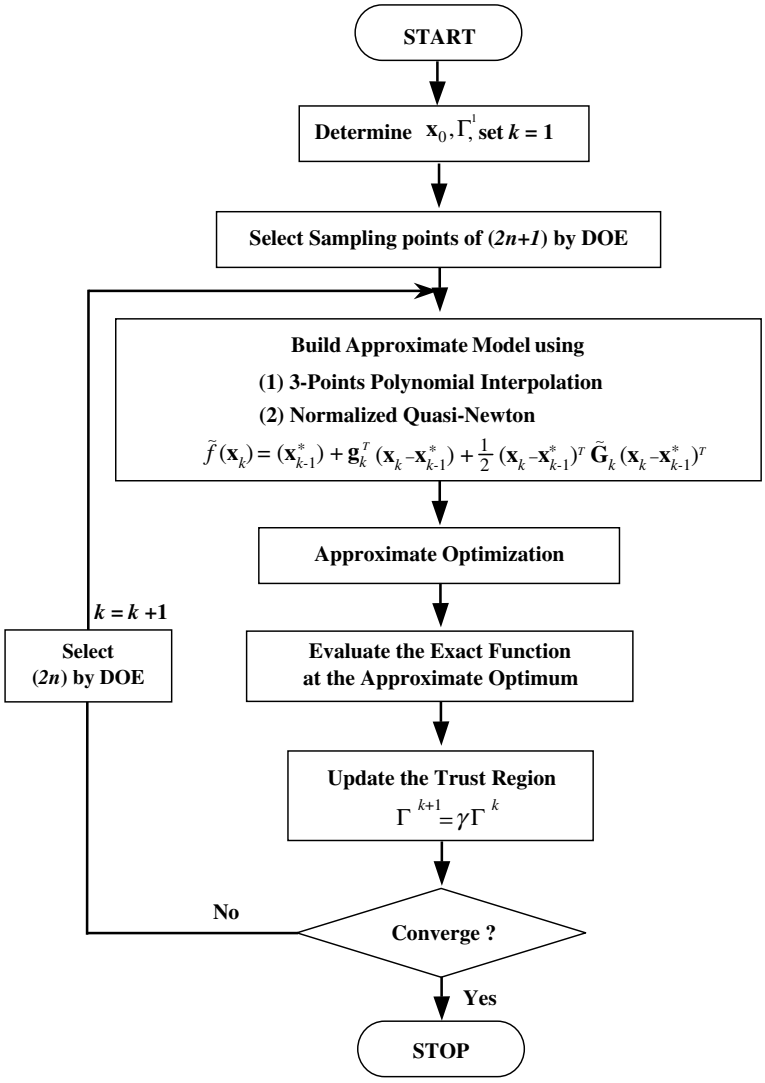

Fig. 5. Computational procedure of the PQRSM.

5. Results and discussion

The optimization problem under consideration in this study is to find the optimal values of the design variables ($\mathbf{x}$) that minimize the pressure drop (ΔP) while the temperature rise (ΔT) is constrained to be less than arbitrarily selected values and the width of a base-part of a fin (B_1) is greater than that of lower-part of a fin (B_2). The plate-fin type heat sink has the fin-to-fin spacing of 7.52 mm and the number of fin is 24. Initially, the fins have a 2 mm width for base-part, a 1.5 mm width for lower-part, and a 7 mm for base thickness, that is, the baseline (initial) geometry of heat sink is $\mathbf{x}_0 = [B_1, B_2, t; 2.0, 1.5, 7.0]$. The optimization problem can be rewritten as the following expressions:

$$\text{Find} \quad \mathbf{x} = [B_1, B_2, t] \tag{21}$$

$$\text{to minimize} \quad \tilde{f}(\mathbf{x}) = \Delta P \tag{22}$$

$$\text{s.t.} \quad g_1 = \frac{\Delta T}{(33\text{K} \sim 36\text{K})} - 1 \leqslant 0 \tag{23a}$$

$$g_2 = \frac{B_2}{B_1} - 1 \leqslant 0 \tag{23b}$$

$$1.25 \leqslant B_1 \leqslant 5.0 \text{ mm}, \quad 1.25 \leqslant B_2 \leqslant 5.0 \text{ mm}, \quad 7.0 \leqslant t \leqslant 25.0 \text{ mm} \tag{23c}$$

5.1. Parametric studies

The effect of each design variable on the pressure drop and the maximum temperature is examined by varying only one variable among the design variables before the optimization is carried out. The parametric studies (i.e., the degree of importance of each design variable) are commonly performed in order to find the most important design variable in a heat sink performance and to choose the most appropriate optimization algorithm by analyzing the distribution of design variables.

The maximum temperature and the pressure drop for various base-part fin widths (B_1) ($1.25 \leqslant B_1 \leqslant 5.0$ mm) are shown in Fig. 6. In this case, the other design variables are fixed as the baseline geometry, i.e., $B_2 = 1.5$ mm and $t = 7.0$ mm ($\mathbf{x} = [B_1, 1.5, 7.0]$). It is noted that the maximum temperature occurs at the bottom surface of the rear heat source. (Heat Source_2, $Q_2 = 321$ W in Fig. 2.) As the base-part fin width increases, the maximum (or junction) temperature decreases, while the pressure drop increases. These phenomena result from the following reasons; for a fixed volume of the heat sink ($L_H \times W_H \times H_H$ = constant), as B_1 increases, the fluid flows fast through channels which are formed by adjacent fins. The increased velocity tends to retard the development of the thermal boundary layer and results in the thinner thermal boundary layer thickness. It also causes to increase the friction loss, which is dependent on the pressure drop. Thus, both the heat transfer rate and the pressure drop are increased as B_1 is thickened. By considering the variations of the maximum temperature and the pressure drop, we can predict from Fig. 6 that the optimum value of B_1 may be approximately ranged as $2 < B_1 < 4$ mm.

To explain the effect of the lower-part fin width (B_2) on the flow and thermal characteristics in the heat sink, the maximum temperature and the pressure drop between inlet and outlet of the heat sink are investigated for various $B_2(1.25 \leqslant B_2 \leqslant 5.0$ mm) and presented in Fig. 7. As can be seen in Fig. 7, the trends in the maximum temperature and the pressure drop are similar to those of Fig. 6 (which is shown about the effects of B_1), that is, as B_2 increases T_j reduces slightly, while ΔP increases linearly. These are due to the same physical reasons as discussed in Fig. 6. Comparing Fig. 7 with Fig. 6, it is obvious that the influence of B_2 on the thermal performance of the heat sink is less significant than that of B_1 (that is, the variations of maximum temperature for B_2 and B_1 are 4.4 K and 6.1 K, respectively, within their ranges). On the contrary, the variations of pressure drop for B_2 and B_1 are estimated as 79.38 Pa and 55.59 Pa, respectively, and it can be concluded that the effect of B_2 on the hydraulic performance is greater than that of B_1 It is also found from Fig. 7 that the optimum value of B_2 according to the constrained conditions would be ranged between 1.25 (lower limit value) and 3.0 mm.

Fig. 8 presents the effect of the base thickness of heat sink ($7.0 < t < 25$ mm) on the maximum temperature and the pressure drop. The pressure drop increases linearly with a small slope as the base thickness increases. An interesting phenomenon can be found for the maximum temperature. As the basement of the heat sink is thickened, the maximum temperature decreases sharply to $t = 15$ mm at which it has a minimum value, and then increases slightly with a further thickened base thickness. Heat generated in the heat sink is removed both by conduction and convection. From the viewpoint of conduction, increasing the base thickness should transfer more heat. However, as shown in Fig. 8, when t is greater than 15 mm, the heat transfer is decreased (i.e., the maximum temperature is increased). This is due to the fact that contact surfaces between fins and cooling air are decreased although the flow velocity induced by the fan becomes greater. In other words, for the case of $t > 15$ mm heat dissipated by conduction increases

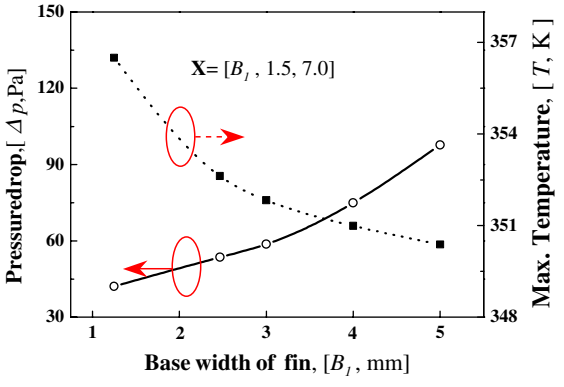

Fig. 6. Effect of base-width of fin on objective functions at $\mathbf{x} = [B_1, 1.5, 7.0]$.

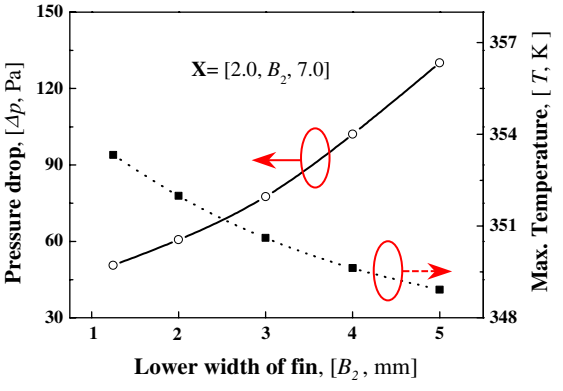

Fig. 7. Effect of lower-width of fin on objective functions at $\mathbf{x} = [2.0, B_2, 7.0]$.

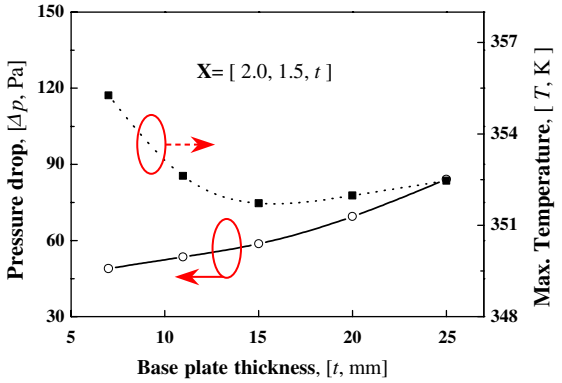

Fig. 8. Effect of basement thickness on objective functions at $\mathbf{x} = [2.0, 1.5, t]$.

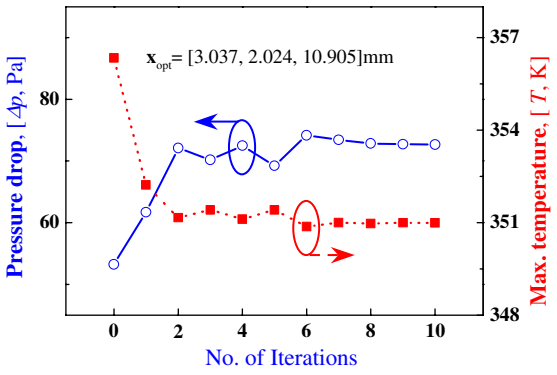

Fig. 9. Convergence histories of pressure drop and maximum temperature for $\Delta T < 33$ K.

continuously, while less heat is transferred by convection. From this phenomenon, it can be explained that for $t > 15$ mm, the base thickness of heat sink (t) adversely affects on the performance of heat sink. Comparing with the results of parametric studies, the effect of t on the thermal performance of heat sink is very small compared to other variables. Moreover, Fig. 8 shows clearly that the optimal values for the base thickness will be smaller than 15 mm irrespective of the required temperature rises.

The parametric studies discussed above show that the pressure drop and maximum temperature in the heat sink are mainly influenced by the fin widths (B_1 and B_2), while the effect of base thickness (t) is relatively small. It can also be found in Figs. 6–8 that the objective function according to the fin widths simply increases or decreases. However, we can find the computational noise and the conversion point for the maximum temperature from Fig. 8, which is shown by the effect of t. The parametric studies also offer important information for optimization that the gradient-based optimization technique like the SQP method may mislead the optimal values. It means that the PQRSM, one of the global optimizations, becomes an effective optimization algorithm rather than the local optimization within the scope of this study.

5.2. Optimal design

The optimum design variables can be obtained by minimizing the pressure drop subjected to two constrained conditions ($\Delta T < 33$–36 K and $B_1 > B_2$) in the heat sink. In this study, the initial pressure drop for the baseline geometry (ΔP^0) is calculated as 53.23 Pa.

Fig. 9 shows the convergence histories for pressure drop and maximum temperature during optimization. In this case, the temperature rise (i.e., one of the constrained conditions) is fixed under 33 K and the optimal values of the design variables obtained are $B_1 = 3.037$ mm, $B_1 = 2.0243$ mm and $t = 10.905$ mm. As shown in Fig. 9, the pressure drop has a sharp increase initially and the optimization process is finished after ten iterations.

To explain the typical results for optimization, the initial (baseline) and optimal designs for the temperature rise of 35 K are listed in Table 1. When minimizing the pressure drop in the heat sink, the value of temperature rise, which is the most important operating factor for thermal stability of heat sink, should be restricted. Otherwise, ΔT (or T_{max}) will tend to continuously increase in excess of its limiting value. As shown in Table 1, for the baseline model, the temperature rise of 38.34 K exceeds the general desired temperature rise of 35 K which is corresponding to the maximum temperature for a safe operation of thermal systems. This means that the plate-fin type heat sink must be optimized for thermal stability. Table 1 also illustrates that the optimized thermal resistance of 0.052 K/W represents a reduction of 8.4% compared to the initial thermal resistance of 0.057 K/W due to the decrease of a temperature rise. In addition, the pressure drop for the optimal design variables is also decreased by 3% from 53.23 Pa to 51.67 Pa. Generally, the improvement of the heat sink

Table 1
Baseline (Initial) and optimized designs for $\Delta T < 35$ K

	Baseline	Optimum
Base-part fin width*, B_1	2.0 mm	2.611 mm
Lower-part fin width*, B_2	1.5 mm	1.267 mm
Base plate thickness*, t	7.0 mm	10.541 mm
Fin height, h	53.0 mm	49.459 mm
Thermal resistance (θ_j)	0.0573 K/W	0.0522 K/W
Pressure drop (ΔP)	53.23 Pa	51.67 Pa
Max. (or junction) temperature (T_j)	356.34 K	352.98 K
Temperature rise (ΔT)	38.34 K	34.98 K

performance can be checked by the thermal performance factor (TPF, η) which is defined as follows;

$$\eta = \frac{(Nu/Nu_{ref})}{(f/f_{ref})^{1/3}} \tag{24}$$

where Nu is the Nusselt number concerned with the maximum temperature and f the friction coefficient that is related to the pressure drop. The subscript ref is the initial condition. When η is greater than 1(one), it means that the thermal performance of the heat sink is improved compared to that of the initial design. We can estimate it by qualitatively. That is, the decrease in the maximum temperature of optimal solutions implies an increase in the heat transfer rate. The reduction of the pressure drop means the decrease in the friction coefficient compared to those of the initial condition. From these results, it can be illustrated that the performance of the heat sink is improved after the optimization. It can also be seen from Table 1 that the optimal values of all design variables, i.e., the base-part fin width (B_1), lower-part fin width (B_2), and base thickness (t) are changed. Note that the optimal values and the corresponding pressure drop depend on the required temperature rises.

The optimal solutions for various desired temperature rises (i.e., $\Delta T = 33$, 34, 35, and 36 K) are presented in Table 2. It enables the comparison of each optimal solution for four different temperature rises. Optimal results for the SQP method [15] are also presented in Table 2 in order to investigate the accuracy of the PQRSM. The objective function for the PQRSM has a lower value than that for the SQP method for all temperature rises as shown in Table 2. For example, for $\Delta T < 35$ K, the objective function (i.e., pressure drop) obtained by the PQRSM is 51.67 Pa and it is lower by 1.87 Pa than that of the SQP method (i.e., 53.54 Pa). The reduction of 3.5% in the pressure drop means that the optimal values by the PQRSM are more accurate than those of the SQP method. Therefore, it is clear that the PQRSM is superior to the SQP method within the range of this study. In Table 2, the "NFC" is the "No. of function calls" and it implies the total number of flow and thermal analyses required (i.e., total number of changes of design variables proposed by an optimizer) throughout the optimization process. However, Table 2 shows that more NFC is needed to obtain the optimal values using the PQRSM. The increased NFC is mainly due to the fact that the optimal values for the PQRSM are global one, while the results for SQP method are a local optimum, which is one of the various optima. Table 2 illustrates that the more heat is removed, the more iterations for obtaining the optimal solutions are needed (for example, for $\Delta T = 33$ and 36 K, the number of function calls are 48 and 32, respectively). This means that if the designer chooses a larger ΔT, the optimizer can easily find the optimal design variables for minimizing the pressure drop during the optimization process. The design variables can be obtained directly from Table 2 for the most useful geometrical configurations of the plate-fins heat sink. That is, if the required temperature rise is 35 K for the safe working in a certain electronic device, a designer simply chooses the design variables in the third column of optimal results in Table 2.

To explain variations of the optimal design variables for four different temperature rises, they are also plotted in Fig. 10. It can be observed that the optimum design variables vary according to the temperature rise (ΔT), as expected. If the value of the required temperature rise is small, large values of B_1 and B_2 will be acquired through the optimization process in order to enhance the heat transfer rate. However, we can observe an interesting result that the variation of optimized base thicknesses (t) with respect to ΔT has a different trend compared to that of other design variables. That is, the base thickness (t) has a maximum value within the optimal solutions. This arises from the following fact; the heat transfer mechanism (i.e., conduction or convection) mainly contributes to dissipating heat for a certain temperature rise condition, as discussed in Fig. 8. From this result, it can be noted that the base thickness has little effect on reducing the pressure drop and increasing the thermal performance. Table 2 and Fig. 10 also show

Table 2
Optimum designs for various temperature rises

	$\Delta T = 33$ K		$\Delta T = 34$ K		$\Delta T = 35$ K		$\Delta T = 36$ K	
	PQRSM	SQP[15]	PQRSM	SQP[15]	PQRSM	SQP[15]	PQRSM	SQP[15]
B_1 [mm]	3.037	2.903	2.961	2.637	2.611	2.468	2.256	2.179
B_2 [mm]	2.024	2.348	1.691	1.897	1.267	1.365	1.250	1.250
t [mm]	10.905	10.491	11.374	10.581	10.541	11.186	9.355	10.041
ΔP [Pa]	***71.23***	72.95	***57.68***	58.21	***51.67***	53.54	***46.22***	47.68
T_j [K]	350.96	350.92	351.91	351.99	352.98	352.99	353.95	353.89
θ_j [K/W]	0.0492		0.0506		0.0522		0.0537	
NFC	48	36	38	33	36	28	32	26

Note: NFC—Number of function calls.

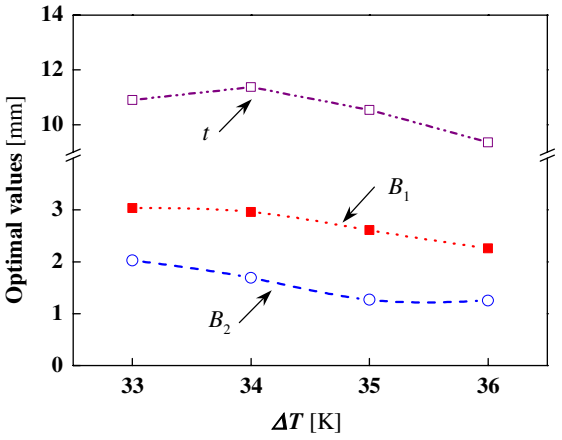

Fig. 10. Optimal solutions for temperature rises (ΔT).

that the pressure drop is decreased with an increase in ΔT. That is, when the temperature rise is increased from 33 to 36 K, the pressure drop is reduced from 71.23 to 46.22 Pa, respectively. The thermal resistances (θ_j) for all temperature rises are decreased compared to that of the initial model (i.e., 0.0573 W/K). Thus, we can find that the performance of the heat sink is improved through the optimal design. In addition, Table 2 illustrates that the pressure drop is inversely proportional to the temperature rise. From this, it is obvious that for design of the heat sink with plate-fins, the choice of the proper design variables is very important by considering which one is preferable between the pressure drop and the thermal resistance (or temperature rise).

A set of optimal solutions for the objective function can be constructed to select the preferred solution based on Table 2. For this, the relationship between the objective function (Δp) and the temperature rise (ΔT) is presented in Fig. 11. The results can be very helpful to designers in order to choose the optimal values of the heat sink. For example, when designers want to focus on decreasing the thermal resistance rather than decreasing the pressure drop, they can select the points such as (*c*) or (*d*) on the curve of Fig. 11 and then can read the corresponding optimal design variables in Table 2. For the thermal management of the heat sink, it is important to remark that the most important goal is to maximize the heat transfer rate or minimize the temperature rise and this is easily achieved both by increasing the velocity in the heat sink and by extending the heat transfer area, as discussed in Figs. 6–8. However, the pressure drop is strongly related to the specific cost, because the size of the fan needed to blow the cool air through the heat sink can be determined by it. Therefore, choosing one of the performance functions (i.e., pressure drop and heat transfer rate) is dependent on the heat sink designers. Finally, it is strongly recommended that the optimal solution of a point (*b*) in Fig. 11 is better than other solutions since both the thermal resistance and the pressure drop are decreased by 8.4% and 3.0%, respectively, compared to those of the initial design. In this case, the optimal design variables are $B_1 = 2.611$ mm, $B_2 = 1.267$ mm, and $t = 10.541$ mm, as shown in Table 2.

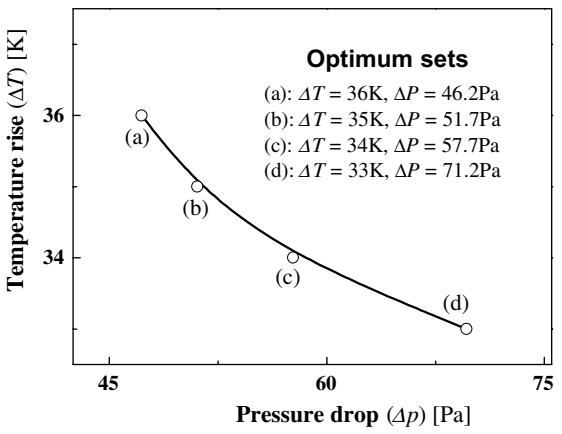

Fig. 11. Relationship between temperature rise (ΔT) and pressure drop (ΔP).

6. Conclusions

The optimal values of the design variables of the plate-fins heat sink to minimize the pressure drop were acquired numerically under the required temperature rise. The thermal and flow characteristics in the heat sink were analyzed using the finite volume method. And the PQRSM method, which is one of the sequential approximate optimization techniques, was used to solve the nonlinear, constrained optimization problem. As the results of optimization, the following conclusions were obtained:

The most dominant design variables for the pressure drop and the thermal resistance were the base-part fin width (B_1), and the lower-part fin width (B_2), while the effect of base thickness (t) on them was relatively small. The optimal design variables could be obtained successively by integration of the CFD code and the PQRSM. The accuracy and efficiency of the PQRSM were validated through the comparison with the SQP method, which is a gradient-based local optimization technique. The results also showed that the optimal design variables for the temperature rise of 35 K were $B_1 = 2.611$ mm, $B_2 = 1.267$ mm, and $t = 10.541$ mm. In this case, both the thermal resistance and the pressure drop for the optimum model were decreased by 8.4% and 3.0%, respectively, compared to those of the baseline model. It was also found that the optimal design variables were varied with the desired temperature rise which is the most important factor for the thermal

stability of heat sink. The optimization could be completed as the relationship between pressure drop and the temperature rise was plotted. The results of this work can offer designers the information they need to select the optimal design variables corresponding to the preferred objective functions.

Acknowledgement

This research was supported by The Center of Innovative Design Optimization Technology (*i*DOT), Korea Science and Engineering Foundation.

References

[1] J.H. Ryu, D.H. Choi, S.J. Kim, Three-dimensional numerical optimization of a manifold microchannel heat sink, Int. J. Heat Mass Transfer 46 (2003) 1553–1562.

[2] K. Park, D.H. Choi, K.S. Lee, Optimum design of plate heat exchanger with staggered pin arrays, Numer. Heat Transfer Part A 45 (2004) 347–361.

[3] K. Park, D.H. Choi, K.S. Lee, Numerical shape optimization for high performance of a heat sink with pin-fins, Numer. Heat Transfer Part A 46 (2004) 909–927.

[4] K. Park, D.H. Choi, Shape optimization of a plate-fin type heat sink with triangular-shaped vortex generator, KSME Int. J. 18 (9) (2004) 867–876.

[5] J.I. Madsen, M. Langyhjem, Multifidelity response surface approximations for the optimum design of diffuser flows, Optim. Eng. 2 (2001) 453–468.

[6] J.F. Rodriguez, J.E. Renaud, B.A. Wujek, R.V. Tappeta, Trust region model management in multidisciplinary design optimization, J. Comput. Appl. Math. 124 (2000) 139–154.

[7] K.J. Hong, M.S. Kim, D.H. Choi, Efficient approximation method for constructing quadratic response surface model, KSME Int. J. 15 (7) (2001) 876–888.

[8] K.J. Hong, M.S. Kim, D.H. Choi, Progressive quadratic approximation method for effective constructing the second-order response surface model in the large scaled system design, J. KSME, Part A 24 (12) (2000) 3040–3052 (Korean).

[9] R. Fletcher, An algorithm for solving linearly constrained optimization problem, Math. Prog. 2 (1972) 133–165.

[10] G.N. Vanderplaats, Numerical Optimization Techniques for Engineering Design with Application, McGraw-Hill, New York, 1984, Chapter 2.

[11] W. Rodi, Turbulence Models and Their Applications in Hydraulics—a State-art-of Review, Book Publication of International Association for Hydraulic Research, Delft, Netherlands, 1984.

[12] K. Abe, T. Kondoh, Y. Nagano, A two-equation heat transfer model reflecting second-moment closures for wall and free turbulent flows, Int. J. Heat Fluid Flow 117 (1996) 228–237.

[13] FLUENT 6 User's Guide, FLUENT Inc., Lebanon, New Hampshire, 2003.

[14] S.V. Patankar, Numerical Heat Transfer and Fluid Flow, Hemisphere, Washington, 1980.

[15] K. Park, D.H. Choi, K.S. Lee, Design optimization of plate-fin type heat sink for thermal stability, in: Proceedings of KSME 2003 Fall Annual Meeting (B), 2003, pp. 43–48 (Korean).